Water Resources Management (2022) 36:1879–1895
https://doi.org/10.1007/s11269-022-03113-4

Permeable Asphalt Hydraulic Conductivity and Particulate Matter Separation With XRT

Mariana Marchioni[1] · Roberto Fedele[1] · Anita Raimondi[1] · John Sansalone[2] · Gianfranco Becciu[1]

Received: 24 September 2021 / Accepted: 11 March 2022 / Published online: 23 March 2022

Abstract
Permeable asphalt (PA) is a composite material with an open graded mix design that provides a pore structure facilitating stormwater infiltration. PA is often constructed as a wearing course for permeable pavements and on impervious pavements to reduce aquaplaning and noise. The pore structure of PA functions as a filter promoting particulate matter (PM) separation. The infiltrating flow characteristics are predominately dependent on pore diameter and pore interconnectivity. X-Ray microTomography (XRT) has successfully estimated these parameters that are otherwise difficult to obtain through conventional gravimetric methods. Pore structure parameters allow modeling of hydraulic conductivity (k) and filtration mechanisms; required to examine the material behavior for infiltration and PM separation. In this study, pore structure parameters were determined through XTR for three PA mixture designs. Additionally, the Kozeny-Kovàv model was implemented to estimate k. PM separation was evaluated using a pore-to-PM diameter categorical model. This filtration mechanism model was validated with data from a rainfall simulator. The filtration model provided a good correlation between measured and modeled data. The identification of filtration mechanisms and k facilitate the design and evaluation of permeable pavement systems as a best management practice (BMP) for runoff volume and peak flow as well as PM and PM-partitioned chemical separation.

Keywords Permeable pavement · Stormwater · X-Ray microtomography · Urban drainage

1 Introduction

These impacts generated by the built environs require adoption of stormwater management control systems that mitigates the coupled runoff volume/flow and loads (Shepherd 2005, Marchioni and Becciu 2014, Tansar et al. 2022, Li et al. 2017, Tsihrintzis and Hamid 1997). Such systems are catorgorized as Sustainable Urban Drainage Systems (SUDS) or LID (Low-Impact Development). Permeable pavement (PP) is categorized as a

✉ Mariana Marchioni
mariana.marchioni@polimi.it

[1] D.I.C.A, Politecnico Di Milano, Milan, Italy

[2] ESSIE University of Florida, Gainesville, USA

SUD or LID and as passive green infrastructure system mitigating runoff volume, flow as well as PM and PM-associated chemical loads (Marchioni and Becciu 2014; Kuang et al. 2015; Ranieri et al. 2010; Ranieri et al. 2017a, b). Hydrologic mechanisms provided by PP include infiltration, evaporation and detention storage with the pore volume and porosity of the PP and base material. The PP surface retains PM as a "schmutzdecke" layer or within the pore structure of PP, thereby sequestering PM and PM-partitioned chemicals for later recovery by maintenance practices such as street sweeping and vacuuming (Ying and Sansalone 2010). PA is often used as a wearing course for PP; supporting vehicular traffic while acting as a passive stormwater control. PA is also implemented as a wearing course for conventional impervious roadways to reduce aquaplaning and noise (Marchioni and Becciu 2015, Poulikakos et al. 2013).

1.1 Flow Through Permeable Porous Media

The pore structure of PA consists of a heterodisperse distribution of pores, and depending on the mix design and pavement construction, of large interconnected pores of equivalent diameters ranging from 2 to 8 mm (Kia et al. 2017; Lu et al. 2020).

Nominally, porosity (ϕ) can be defined as the fraction of the unit volume occupied by all pores. Total or absolute porosity (ϕ_T) represents the fraction of all the pores within the volume of the material while effective porosity (ϕ_e) considers only the fraction of pores that are interconnected across the depth of the PP and transmit flow. ϕ_e can be indexed to k (Collins 1976). For PP types such as pervious concrete and PA, ϕ_T typically ranges from 0.15 to 0.35 (Lu et al. 2020; Tennis et al. 2004). For PP the porosity can be determined by direct methods as density methods (Tennis et al. 2004; Montes et al. 2005; CEN ECfS 2012). XRT can be used to obtain ϕ_T, ϕ_e and pore particle size distribution (PSD_{pore}) otherwise difficult to obtain with traditional methods (Kuang et al. 2015; Chen et al. 2020; Huang et al. 2020; Lu et al. 2020).

Hydraulic conductivity (k) is a quantitative measure of the transmission of fluid (in most PP conditions, water) through a permeable matrix with the fluid subject to an applied hydraulic gradient. To represent k, the sample or specimen tested must be sufficiently large to contain many pores in a representative elemental volume (Collins 1976). A measure of k depends on pore structure, effective porosity, tortuosity, pore size distribution and shape of the pores. Also, k is a function of construction, compaction and mechanical alterations of the PP structure (Kia et al. 2017; Collins 1976; Kuang et al. 2015). The pore structure of the PP surface has a critical impact on k. A determination of k can be measured with direct methods in laboratory, using falling head or constant head permeameters, or in situ, normally using infiltrometers that use the principle of the falling head permeameter (Ranieri et al. 2012; Terzaghi et al. 1996; Collins 1976). K can also be measured by indirect methods using pore parameters (Ranieri et al. 2010; Terzaghi et al. 1996). The theory of Kozeny relates the pore structure to k by considering a permeable matrix as a bundle of straight capillary tubes and then considering a solution using hydrodynamic equations for slow and steady flow. The equation resulting from Kozeny was later modified to include the concept of tortuosity, considering that the tubes of flow are not straight (Collins 1976). Using a modified Kozeny-Kovàv model (KKM) as shown in Eq. (1) (Ranieri et al. 2010) compared measured and modeled saturated hydraulic conductivity (k_{sat}) results. The modified equation introduces the ϕ_e instead of ϕ_T considering thus the effective porosity that effectively contributes to k.

$$k_{sat} = \frac{1}{512}\frac{\gamma}{\eta}\varnothing_e D_e^2 \quad (1)$$

In this equation, γ is the water specific weigh, η is the dynamic viscosity, ϕ_e is the effective porosity and D_e is the characteristic diameter. Ranieri et al. (2010) compared the results of measured k_{sat} with modeled using different diameter indices D_e (D_5, D_{10}, D_{15}, D_{20}, D_{30}, D_{40}, D_{50} and D_{60}) and found the best fit when using the D_{30} to evaluate k_{sat} which was measured using a constant head permeameter.

1.2 Runoff PM Load

Generation and deposition of PM by anthropogenic activities plays an important role in the partitioning, distribution and fate of chemicals in urban areas. Heterodisperse PM generated by anthropogenic activities, predominately traffic and urban activities function as a vector and labile reservoir for chemical loads transported by runoff (Tsihrintzis and Hamid 1997). PM and chemicals from anthropogenic activities are accreted on or adjacent to impervious paved surfaces (the buildup phase) until washoff phase by hydraulic stress of runoff. The chemical load partitions to/from PM and distribute across the particle size distribution (PSD) (Ying and Sansalone 2010; Liu et al. 2014). PM poses as a health risk, especially the finer fraction (< 10 μm), in particular PM < 2.5 μm (European Commission 2008, IARC Working Group on the Evaluation of Carcinogenic Risks to Humans 2016). Vehicular traffic activities is a main source for dry deposition PM from vehicular and pavement abrasion. This PM can range from gravel- to sub-micron size and has been correlated with indices such as average daily traffic (ADT), wind speed/direction. The accreted surface PM load can be further abraded by traffic into finer PM sizes (Sansalone et al. 2009). Metals (Cd, Cr, Cu, Fe, Ni, Pb and Zn), nutrients and organic chemicals are constituents that partition and distribute across the PSD as a function of the constituent chemistry, and the particle size total surface area and charge. (Sansalone et al. 2009). By definition, the suspended fraction (< 25 μm) has the highest concentration of metals [mg/kg of dry PM] and is highly mobile in runoff and not retained by BMPs and is most bio-available. In contrast the sediment fraction (> 75 μm) which is the dominant mass fraction (and therefore has the predominant total surface area) transported in runoff is the PM substrate of the highest total metal mass, is readily separated in urban conveyance systems and BMPs yet is the most labile fraction (Ying and Sansalone 2010; Sansalone et al. 2009; Sansalone and Ying 2008; Sansalone and Cristina 2004; Deletic and Orr 2005). PP can function as a filter for near-source control to separate PM and PM-partitioned chemicals from runoff. PSDs of dry deposition PM and PP pore geometric parameters are essential to design control strategies for management of PM and PM-partitioned chemicals. If the PP is pervious concrete (in contrast to PA) the pore geometrics and surface chemistry also provide surface complexation and chemical precipitation mechanisms for metals and phosphorus. While the PM filtered by PP, whether as a schmutzdecke or deep bed deposit does act as a substrate for surface complexation, these PM reservoirs are potentially mobile unless recovered by regular maintenance and the deep bed filtered PM predominately impacts the driving head through the PP.

The dry-deposition and runoff PM median diameter (D_{50}), where 50% of particles are finer by mass, for different studies ranges from 100 to 1100 μm (Deletic and Orr 2005; Ranieri et al. 2017a; Sansalone et al. 2009; Zhang and Sansalone 2014; Sansalone and Ying 2008; Ying and Sansalone 2010; Sansalone and Tribouillard 1999; Ranieri et al. 2017a, b;

Dickenson and Sansalone 2012; Zhang and Sansalone 2014). The D_{50} of runoff (Zhang and Sansalone 2014; Ying and Sansalone 2010) was smaller than that obtained with dry deposition (154 µm versus 280 µm; 331 µm versus 97 µm). This difference indicates that runoff does not necessarily deliver the coarser PM fraction of the gradation, depending on the hydraulic stresses. This coarser PM is then available for abrasion by traffic. Deletic and Orr (2005) used a wet method of sampling by washing and then vacuuming to capture the suspended PM. The mean D_{50} and D_{10} over the period of a year was 397 µm and 34 µm. The D_{50} varies also with the sample position where larger particles are found mainly on the road shoulders and are more mobile with higher hydraulic stresses of runoff.

1.3 Filtration Mechanisms

The PP pore mean diameter (d_m) and PM particle diameter (d_p) are parameters to identify particle filtration mechanisms. Three main mechanisms of transport can be distinguished: formation of a schmutzdecke also known as a surface (cake) generated by surficial straining, deep-bed filtration within the pore space leading to a reduction in porosity, and physical–chemical filtration where the fine suspended PM attaches to the pore surfaces in the PP but do not generate a significant reduction in porosity. When the particles are relatively large compared to the media the particles does not penetrate and are retained on the surface forming a cake or a *schmutzdecke*, translated as "dirty layer" in German (Teng and Sansalone 2004). This cake increases in thickness over time and can potentially function as a hydraulically resistant filter, reducing the system infiltration yet al.so acting as a substrate for chemical surface complexation. This potential mechanism has been indexed at a $d_m/d_p < 10$ (McDowell-Boyer et al. 1986). However, the cake is potentially protective to mitigate deep-bed filtration and is easily recovered by conventional maintenance practices.

Deep-bed filtration, is a result of a series of potential separation mechanisms of particles within the pore distribution of PP, occurs is a narrower range of approximately $10 < d_m/d_p < 20$, and plays an important role in PM and chemical separation, albeit with filter ripening, increased head loss and failure without regular maintenance (Auset and Keller 2006, McDowell-Boyer et al. 1986). Smaller particles can only be removed by physical–chemical filtration mechanisms, normally when $d_m/d_p > 20$. In this case the mechanism depends basically on the particle diameter, whereas particles with $d_p > 5$ µm are still subject to the effect of gravitational sedimentation, and $d_p < 5$ µm the effect of Brownian motion. These mechanisms have been identified for PP including pervious concrete (Teng and Sansalone 2004).

2 Objectives

In this research XRT was implemented to obtain pore structure parameters (ϕ_T, ϕ_e, PSD_{pore}) on permeable asphalt (PA) specimens. With these parameters and measured data, k was examined using the Kozeny-Kovàv model (KKM). The primary PM separation mechanisms were then evaluated with a categorical model. This mechanistic filtration model was used to estimate the PM fate for the PA specimens examined relating the pore structure obtained with XRT and the PSD_{PM} comparing the results with data measured in the laboratory using a rainfall simulator. The PM loads considered were assembled based on laboratory and field-based sampling. The modeled PM separation was validated with measured data using the rainfall simulator.

3 Materials and Methods

3.1 Laboratory Rainfall Simulation

PA specimens were produced in the laboratory with dimension of 50×26×5 cm and 0.15. 0.20 and 0.25 nominal total porosity (ϕT,Nominal). A rainfall simulator was designed to investigate the PM fate on porous surfaces (Andrés-Valeri et al. 2016; Brugin et al. 2017; Marchioni et al. 2021). Aerial PM loading with concentrations of 0.5 kg/m^2, 1.0 kg/m^2 and 2.0 kg/m^2 were applied on the specimens that were subject to rainfall events of 50 mm/h, 100 mm/h, 150 mm/h intensities with 15-min duration and rainfall intensity of 100 mm/h with 30 min duration. The device collected superficial runoff and infiltrated water that were then over dried to gravimetrically quantify the PM in these flow streams. In the case of infiltrated water, due to the large volume, the measure was made by collecting three samples of the total volume and then integrating across the total volume.

3.2 Particulate Matter (PM) Loads

To simulate dry deposition of PM loads in the rainfall simulation tests a mix of quarry sand and recovery fillers was assembled with a particle size distribution $(PSD)_{PM}$ that replicates real dry deposition ranging from 75 to 2000 µm and a small silt-size fraction. Traffic dry deposition PM samples were also collected on four asphalt-paved roadways in Milan (Italy). The four roads are constructed of impermeable asphalt in a highly inhabited mostly residential zone, and the samples were collected in October and November 2016 (autumn season) in the evening before cleaning. The method used was manual sweeping on the paved road shoulders to avoid fine particles loss that might happen with vacuuming. The PSD_{PM} for the laboratory assembled mix and field samples was obtained through mechanical sieve analysis according to UNI EN 933–1. For each particle size distribution, it was determined the indices D_{10}, D_{50}, D_{60}, D_{90}, as the percent of particles finer than 10, 50, 60 and 90% and the uniformity coefficient according to Eq. (2). The cumulative mass $(PSD)_{PM}$ was modeled as a cumulative gamma distribution. The goodness of fit was verified using the Kolmogorov–Smirnov (k-s) statistics test with $p > 0.05$. The Kruskal–Wallis test with $\alpha = 0.05$ significance level was used to verify if the four different samples were statistically significantly different.

$$U = \frac{d_{60}}{d_{10}} \tag{2}$$

3.3 XRT Analysis

XRT analysis implemented to investigate pore parameter of granular media and PP is well documented in the literature (Teng and Sansalone 2004; Sansalone et al. 2008; Kuang et al. 2015; Chen et al. 2020; Huang et al. 2020; Lu et al. 2020). This study employed a XRT NSI X25 system (NSI Inc., Rogers, MN, USA) available at Politecnico di Milano, equipped with a Dexela detector with 75 µm pixel pitch allowing for the acquisition of 1536×1944 pixel radiographies at full-binning with 16 bit encoding. Samples (10×10×5 cm) extracted from the PA specimens, molded in the laboratory and representing each porosity, were scanned.

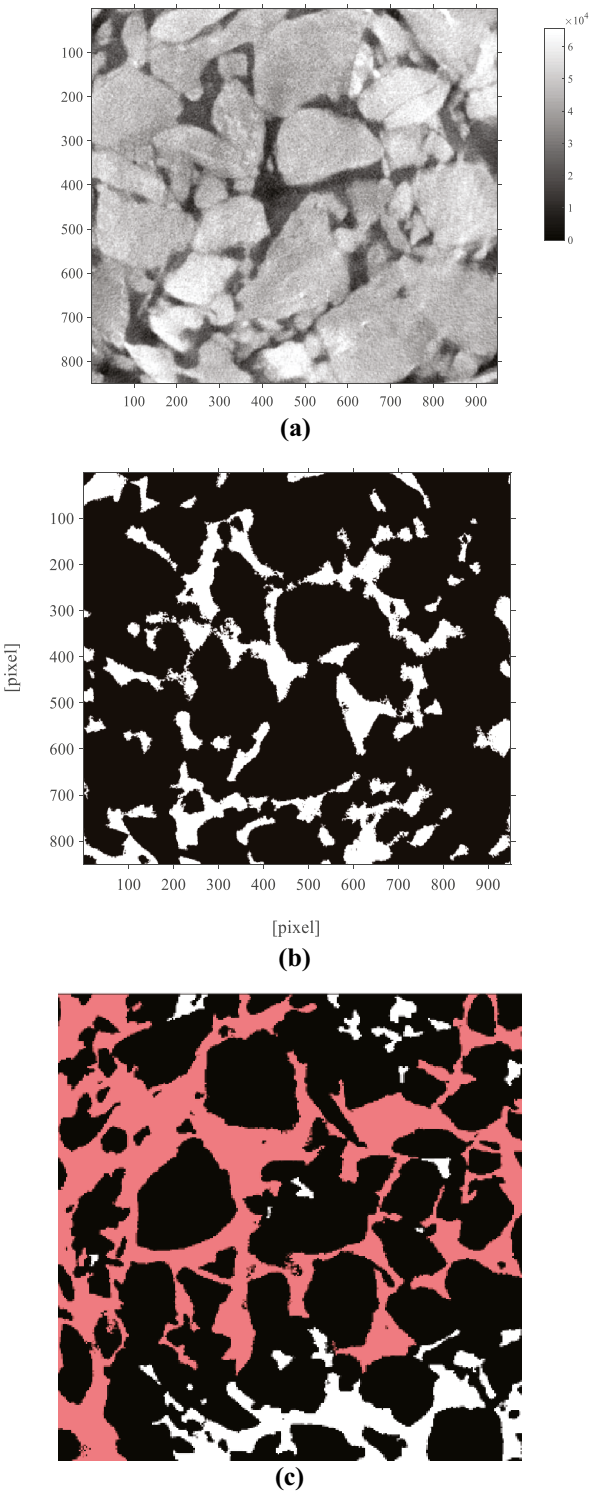

Fig. 1 (**a**) Original image acquired with the XRT and (**b**) binary image used in the analysis, where the white pixels represent the pores, (**c**) pore identification for a sample layer

The X-ray beam was set to 110 kVp (kilovoltage peak.[116,117]) and 48 μA, and a frame-rate of 6.6 Hz was adopted together with a 13 frame-averaging (to reduce noise), leading to 1800 angular projections. From the cone-beam geometry, the estimated voxel size was 61.88 μm with a zoom-factor equal to 1.21. Three dimensional (3D) tomographic reconstruction was performed using a modified Feldkamp algorithm in the version provided by X-CT commercial software (NSI Inc.) (Fedele et al. 2013). The 3D reconstruction required approximately 2.5 h were required on a Work Station HP Z820 with 8 CPUs INTEL XEON© E52630 @2.6 GHz, and NVIDIA GPU GeFOrce GTX 80 Ti.

3.4 Digital Image Processing

For each sample approximately 800 images (requiring 8 Gigabyte storage) per cartesian plane (XY, XZ, YZ) were obtained. The pore structure parameters were obtained for the XY cartesian plane with respect to the nominal direction of infiltrating water flow from the laboratory rainfall simulation tests. All images were processed in a Matlab R2016a environment. The image processing consisted of first adjusting image contrast to improve pore identification. The 16-bit greyscale images where binary (black and white images), where the solid pixels (white) represented the matrix and the black pixels represented the pores (air voids). In order to measure the pores, the black and white pixels were inverted such that the solid pixels (white) represented the pores. The last step was to remove any noise, define as pores with less than 100 pixels, that could influence results as shown in Fig. 1.

3.5 Pore Parameters

The pore parameters of total porosity ($\phi_{T,XRT}$), effective porosity (ϕ_e), equivalent pore diameter, $PSD_{(pore)}$ were evaluated to examine the response of the permeable matrix to the transport of fluid, solute and PM loading as demonstrated in the literature (Kuang et al. 2015). To obtain these parameters after image processing, the next operation was to identify each pore per image by identifying a solid pixel p and use a flood-fill algorithm, an algorithm that determines and alters the area connected to a given pixel p in a multi-dimensional array, labeling all the pixels connected to p. Each group of connections represents a pore. In Fig. 1 a single pore is identified with a pink color, to illustrate a sample of high connectivity.

The total porosity obtained with XRT ($\phi_{T,XRT}$) was calculated according to Eq. (3), where v_c indicates the volume for each pore, obtained by weighting on a volume basis all pores in each connection, v denotes the total volume and m is the total number of pores.

$$\varnothing_{T,XRT} = \frac{\sum_{i=1}^{m} v_{ci}}{v} \tag{3}$$

Table 1 Sampling sites

Sample ID[(a)]	Street	Date of sampling	Land use
MI_golgi_17_ott_2016	Via Golgi	17/10/2016	Residential
MI_pascoli_21_ott_2016	Via Pascoli	21/10/2016	Residential
MI_romagna_2_nov_2016	Viale Romagna	2/11/2016	Residential Mostly
MI_zanoia_4_nov_2016	Via Zanoia	4/11/2016	Residential

[a]The samples ID follows the rule city_address_date_month_year. MI stands for Milan

Fig. 2 PSD_{pore} obtained with XRT and image analysis. (**a**) – PA_25_A, (**b**) – PA_25_B, (**c**) – PA_25_C, (**d**)—PA_25_D, (**e**) – PA_15_A, (**f**) – PA_15_B, (**g**) – PA_15_C, (**h**) – PA_20

To calculate the effective porosity (ϕ_e) all the pores that didn't have pixels on the first layer (z = 0) and on the last layers scanned were excluded. Only the connected pores that went all the way through the specimens were considered. The effective porosity was computed according to Eq. (4).

$$\varnothing_{e=\frac{\sum_{i=1}^{m} v_{Cei}}{v}} \tag{4}$$

In this equation v_{ce} is the volume for each effective pore connection, obtained by weighting all the connected pores on a volume basis, v is the total volume of pores and m is the total number of pore connections.

For each pore in each connected region were obtained the volume and the equivalent diameter (d_m), i.e. the diameter of the circumference covering the same area as the pore, and the pore size distribution [$PSD_{(pore)}$]. The pore diameter indexes D_{30} and $D_{50;}$ as the diameter with less than 30% and 50% pores; were also obtained.

The effective porosity (ϕ_e) and pore diameter index D_{30} were used to model k using the modified Kozeny-Kovàcs based on Eq. (1). The pore diameter index D_{50} was used combined with the $(PSD)_{PM}$ to model the particle separation according to the categorical mechanistic model for filtration.

4 Results

4.1 Pore Parameters

The eight PA specimens extracted from the test slabs produced in the laboratory were submitted to XRT and image analysis to obtain the pore structure parameters ($\phi_{T,XRT,}$ ϕ_e, PSD_{pore}) shown in Table 1. The mean relative difference between $\phi_{T,Nominal}$ and $\phi_{T,XRT}$ was 5% and ranged from 4 to 22% while the mean relative difference from $\phi_{T,XRT}$ and ϕ_e was 6% ranging from 1 to 27% indicating a highly interconnected structure that was also visually confirmed.

The mean pore diameter mean ($d_{m,\ mean}$) ranged from 2.27 mm to 2.75 mm with a mean of 2.52 mm and standard deviation of 0.19 when considering all samples of different nominal porosities ($\phi_{T,Nominal}$ of 0.15, 0.20 and 0.25). The results are in agreement with PA equivalent pore diameter found in literature ranging from 0.5 mm to 5 mm (Kuang et al. 2015; Sansalone et al. 2008; Alber et al. 2018; Huang et al. 2020; Chen et al. 2020).. The same mix design and aggregate PSD was used for all specimens explaining the similar results for pore diameter mean for different porosities.

Figure 2 illustrates the PSD_{pore} on pore diameter (d_m) basis for each PA sample as a probability density function (PDF) and cumulative density function (CDF). The d_m ranged from 0.75 mm to 12 mm with a mean D_{50} of 1.88 mm for all samples and D_{90} of 5.25 mm for all samples with the exception of PA_15_A with a D_{90} of 7.25 mm.

4.2 Modeled Saturated Hydraulic Conductivity (k_{sat})

The KKM proposed by Ranieri et al. (2010) was used to determine k_{sat} using the pore diameter (D_{30}) obtained with XRT and image analysis (Table 2). The results ranged from 2.88×10^{-4}

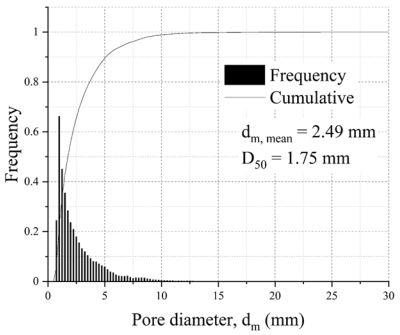
Frequency
Cumulative
$d_{m,mean}$ = 2.49 mm
D_{50} = 1.75 mm
Frequency
Pore diameter, d_m (mm)

(a)

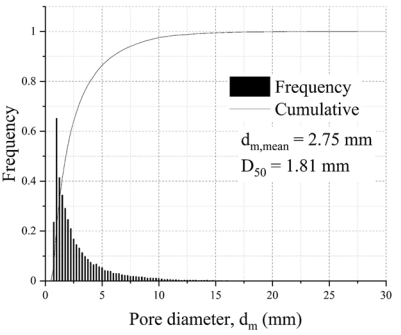
Frequency
Cumulative
$d_{m,mean}$ = 2.75 mm
D_{50} = 1.81 mm
Frequency
Pore diameter, d_m (mm)

(b)

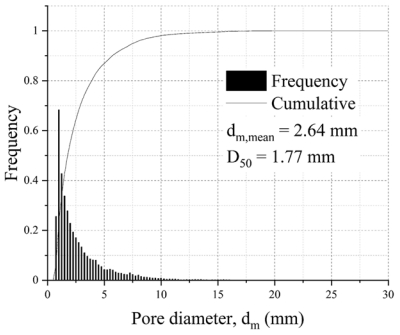
Frequency
Cumulative
$d_{m,mean}$ = 2.64 mm
D_{50} = 1.77 mm
Frequency
Pore diameter, d_m (mm)

(c)

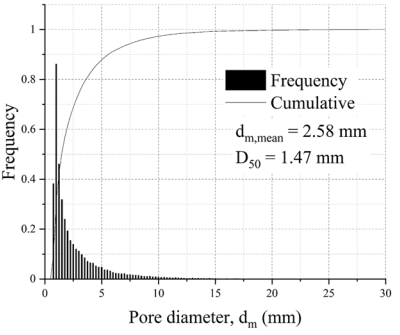
Frequency
Cumulative
$d_{m,mean}$ = 2.58 mm
D_{50} = 1.47 mm
Frequency
Pore diameter, d_m (mm)

(d)

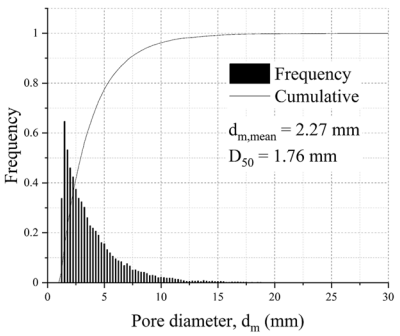
Frequency
Cumulative
$d_{m,mean}$ = 2.27 mm
D_{50} = 1.76 mm
Frequency
Pore diameter, d_m (mm)

(e)

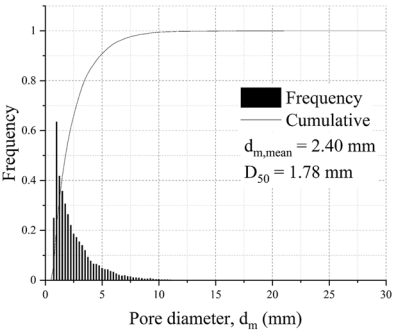
Frequency
Cumulative
$d_{m,mean}$ = 2.40 mm
D_{50} = 1.78 mm
Frequency
Pore diameter, d_m (mm)

(f)

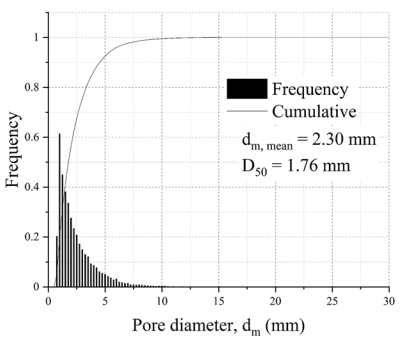
Frequency
Cumulative
$d_{m,mean}$ = 2.30 mm
D_{50} = 1.76 mm
Frequency
Pore diameter, d_m (mm)

(g)

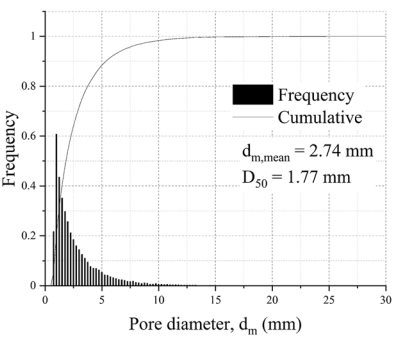
Frequency
Cumulative
$d_{m,mean}$ = 2.74 mm
D_{50} = 1.77 mm
Frequency
Pore diameter, d_m (mm)

(h)

Table 2 Pore structure parameters

Sample ID[a]	Nominal total porosity[b] $\phi_{T,Nominal}$ [-]	Total porosity $\phi_{T,XRT}$ [-]	Effective porosity ϕ_e [-]	Pore area mean A_{mean} [mm^2]	Pore area median A_{median} [mm^2]	Pore diameter mean $d_{m,\,mean}$ [mm]	Pore diameter median D_{50} [mm]	D_{30} [mm]
PA_25_A	0.25	0.2025	0.1977	8.41	2.41	2.49	1.75	1.16
PA_25_B	0.25	0.2260	0.2202	11.74	2.58	2.75	1.81	1.19
PA_25_C	0.25	0.2130	0.2093	10.05	2.45	2.64	1.77	1.15
PA_25_D	0.25	0.2395	0.2367	13.06	1.69	2.58	1.47	0.99
PA_15_A	0.15	0.1344	0.1209	6.38	2.43	2.27	1.76	2.01
PA_15_B	0.15	0.1576	0.1484	7.53	2.48	2.40	1.78	1.16
PA_15_C	0.15	0.1370	0.1006	6.41	2.44	2.30	1.76	1.21
PA_20	0.20	0.2432	0.2472	12.92	2.46	2.74	1.77	1.22

[a]The samples ID follows the rule MATERIAL_NOMINAL TOTAL POROSITY_SAMPLE NUMBER

[b]Obtained with bulk density

Table 3 Modeled saturated hydraulic conductivity, $k_{sat,modeled}$

Sample ID	Effective porosity ϕ_e [-]	D_{30} [mm]	$k_{sat\ modeled}$ (m/s)
PA_25_A	0.20	1.16	5.21×10^{-4}
PA_25_B	0.22	1.19	6.06×10^{-4}
PA_25_C	0.21	1.15	5.42×10^{-4}
PA_25_D	0.24	0.99	4.50×10^{-4}
PA_15_A	0.12	2.01	9.54×10^{-4}
PA_15_B	0.15	1.16	3.91×10^{-4}
PA_15_C	0.10	1.21	2.88×10^{-4}
PA_20	0.25	1.22	7.12×10^{-4}

to 7.21×10^{-4} m/s where the lowest k_{sat} was observed for the specimen with $\phi_{T,Nominal}=0.15$. Soils as granular matrices with hydraulic conductivity within this range are considered having good drainage properties (Terzaghi et al. 1996).

4.3 PM Loads Characteristics

Table 3 shows $(PSD)_{PM}$ results from the PM loads used in the laboratory rainfall simulation tests and collected from the field. D_{50} field values ranged from 524 µm to 1767 µm, higher when compared with previous studies where the mean D_{50} regardless of sampling method was 408 µm and median 351 µm (Table 4 – SI). Comparing the laboratory and field samples using the Kruskal–Wallis test indicated that the five samples did not show a statistically significantly difference between PSDs for a p-value = 0.8892 with 95% confidence level. The gravimetric PSD was modeled as a cumulative gamma distribution with a goodness of fit verified using the Kolmogorov–Smirnov (k-s) statistics test with ($p > 0.05$) (Table 5).

4.4 Measured Particle Separation

PM fate measured from the laboratory physical modeling elucidated the PM mass: retained on the PA specimens (as a schmutzdecke), within the specimens as deep bed filtration (specific deposit), exfiltrated through the specimen, or washed off the specimens through the hydraulic stress of runoff. Figure 3 illustrates the PM fate for PA specimens load with 0.5 kg/m^2 and 2.0 kg/m^2. PM subject to a 100 mm/h rainfall with 30 min duration and 150 mm/h and 15 min duration and also 2.5 and 7.0% slope. The majority (> 85%) of the PM load was retained on

Table 4 PM load characteristics

Sample ID	d_{10} [µm]	d_{50} [µm]	d_{60} [µm]	d_{90} [µm]	U [-]
Laboratory assembled mix	189	1906	3347	9593	18
MI_golgi_17_ott_2016	185	1767	2502	6794	13.5
MI_pascoli_21_ott_2016	75	1150	1732	5954	23.1
MI_romagna_2_nov_2016	75	738	1092	3862	14.6
MI_zanoia_4_nov_2016	89	524	715	1780	8.0

the specimen surfaces as a schmutzdecke and within the pore matrix of the specimens. For the test conditions the schmutzdecke formation did not increase volumetric runoff substantially; remaining below a volumetric runoff coefficient of 0.20 (Andrés-Valeri et al. 2016). Less than 15% was exfiltrated through the specimens and consisted of fine suspended PM. The portion of PM loads that exfiltrated through the specimen could potentially reach subgrade below the PA pavement structure, where the inclusion of a geotextile could retain these exfiltrated particles if required. A nominal fraction of PM (<2% on a gravimetric basis) was washed off with runoff indicating that for the test conditions that the use of PA reduce PM loads that reach the drainage system.

Increasing PM load also increase the PM mass retained on the specimen as the schmutzdecke formed on the surface due to progressive filtration by the schmutzdecke to retain finer suspended PM that otherwise would pass into and through the PA with the potential of exfiltration of suspended PM as PM-partitioned chemicals to subgrade. Given that there was not a significant increase of the runoff PM mass and neither the volumetric runoff coefficient indicates that the schmutzdecke acts to improve the retention of PM without impacting runoff reduction and therefore benefits the permeable pavement service life. By increasing slope or rainfall intensity a slight increase on runoff volume that washed off part of the PM that otherwise would be retained on the specimen, consequently increasing PM mass on runoff. Results of the PM fate on a percent mass basis for different test conditions are available in the SI.

4.5 Modeled PM Separation

The categorical mechanistic model considering that the ratio d_m/d_p governs the PM fate was applied for the laboratory physical model and field PM and compared with the PM fate obtained with the rainfall simulator for validation. The d_m considered was the mean pore diameter ($d_{m,\ mean}$) obtained through XRT for each sample (Table 1) while d_p came from the $(PSD)_{PM}$. For the laboratory PM gradation most of the PM mass (83.1% to 88.5%) was retained on the PA surface forming a schmutzdecke (Table 6). In this scenario the PM is easily recovered through standard maintenance practices such as using vacuuming devices. The percent of mass that was filtered in the pore space through physical–chemical parameters, and therefore could potentially exfiltrate to the subgrade, ranged from 7.6 to 11.3%. The measured and modeled data presented a maximum of 8% of relative percent difference. The simple categorical mechanistic model presented representative results under the test conditions.

The categorical mechanistic model was then applied for the field dry deposition PM samples. For all the PA samples, 87% of the PM mass was retained on the specimen surface creating a schmutzdecke. The percent of PM mass that was retained through deep bed filtration was 5% for the PA_20 (0.20 porosity) 10% for the PA_25 (0.25 porosity) and 8% for the PA_15 (0.15 porosity).

The percent of PM mass that was potentially detained only by physical–chemical mechanism allowing for potential exfiltration was 7% for the PA_20 (0.20 porosity) 3% for the PA_25(0.25 porosity) and 3% for the PA_15 (0.15 porosity). The results depend on the d_m and not on the total porosity which can explain equivalent results for different total porosity and less PM passing through the $\phi_{T,nominal} = 0.25$ porosity specimen than the $\phi_{T,nominal} = 0.15$ specimen. This can also explain the similar results for filtration mechanisms since d_m governed filtration mechanism for the same index of mean pore diameters.

Table 5 Cumulative particle size distribution $(PSD)_{PM}$ modelling parameters

Sample ID	Gamma distribution			Goodness of fit[a]		
	α	**β**	**SSE**	**p-value**	**K-S**	**Hyp. Null[b]**
Laboratory assembled mix	0.59	6.74	102	1.0000	0.0909	true
MI_golgi_17_ott_2016	0.80	3.45	36.35	0.9448	0.1667	true
MI_pascoli_21_ott_2016	0.57	3.89	142.05	0.3874	0.2941	true
MI_romagna_2_nov_2016	0.56	2.57	284.39	0.3874	0.2941	true
MI_zanoia_4_nov_2016	1.09	0.66	307.97	0.3874	0.2941	true

[a]Fit of the cumulative gamma distribution

[b]Null hypothesis that the samples are drawn for identical distribution ($p > 0.05$). True or false

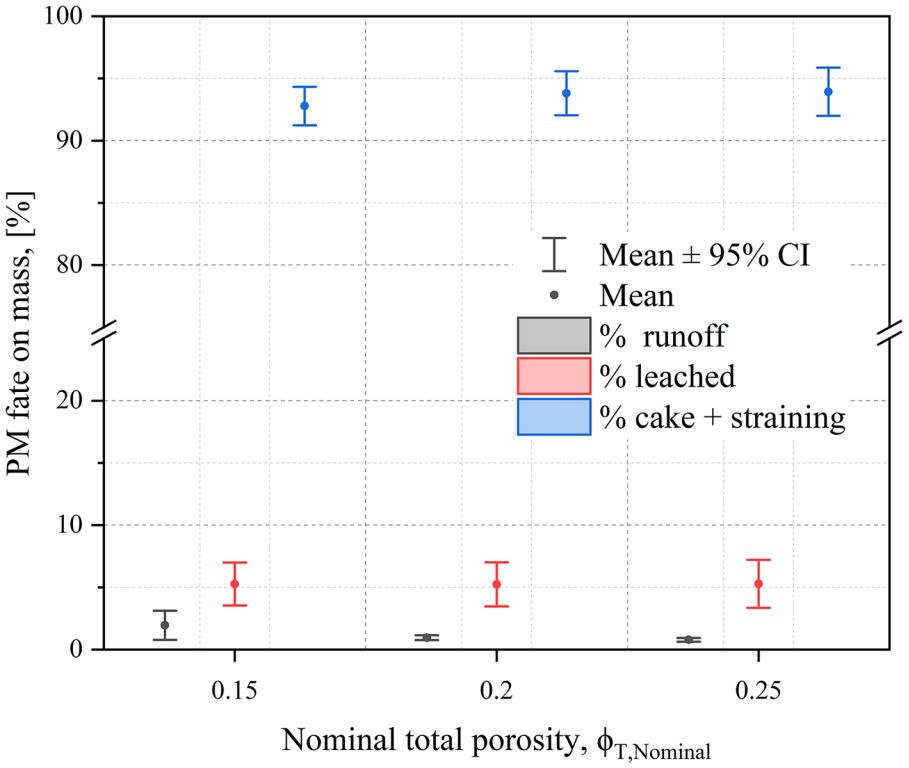

Fig. 3 PM fate on mass for PA specimens for various rainfall and load conditions

Table 6 Modeled dominant filtration mechanism for the laboratory PM assembled mix on mass

Sample ID	PM fate on mass		
	Physical–chemical	**Straining**	**Cake**
PA_25_A	8.4%	4.2%	87.4%
PA_25_B	8.5%	4.3%	87.1%
PA_25_C	8.4%	4.2%	87.3%
PA_25_D	7.6%	3.8%	88.6%
PA_15_A	11.3%	5.6%	83.1%
PA_15_B	8.4%	4.2%	87.4%
PA_15_C	8.4%	4.2%	87.4%
PA_20	8.6%	4.3%	87.0%

5 Conclusions

The continued growth of urbanization requires a comprehensive stormwater management approach emphasizing source control for runoff, PM and chemicals. Such solutions move beyond conventional conveyances of stormwater from one location to another location downstream. PM accumulated on pavement surfaces is mobilized by hydraulic stresses after the PM buildup phase and is transported in stormwater into drainage systems becoming a source of impairment for receiving waters. Permeable pavement systems using permeable surface materials such as pervious concrete and permeable asphalt (PA) provides stormwater infiltration, reducing runoff, and acts as a filter promoting PM and chemical load removal. This type of control system is an established technology that is market-available and amenable to design, regulations and standards. Current research focuses on materials characteristics, modelling and improves overall performance.

This research used a rainfall simulator, X-Ray microTomography (XRT) and field material sampling to investigate aspects of PM separation by PA. Pore structure parameters (total porosity, effective porosity, pore size distribution) that are complex or not possible to obtain through conventional methods were obtained through XRT. Once a methodology was established for image analysis obtained with XRT these parameters were quantified. However, the method is still a research method and needs further development for applications outside of the research environment. The ϕ_T results were in accordance with the results obtained through bulk density. The ϕ_T and ϕ_e, both obtained through XRT, presented a mean relative difference of 6% and results were confirmed by visual observation of the highly interconnected pores.

The modeling of hydraulic conductivity (k) results confirmed that the PA samples are suitable to allow stormwater infiltration providing k values similar to a well-drained granular soil. The filtration mechanisms were investigated by physical modeling and using a categorical mechanistic model based on pore and particle diameter. For the specimens studied and imposed loadings the dominant mechanism was the PM accumulation on the surface, namely a schmutzdecke or surface cake of PM which provided progressive filtration and protection of the PA pore space. Most of PM (> 85%) remained on the porous surface with a much smaller fraction subject to deep-bed filtration for both the laboratory PM mix and the samples obtained on field. This "cake" leads to a nominal

k reduction while functioning by also retaining finer suspended PM over time that otherwise would pass through and potentially be exfiltrated from the PA. Hence, as the schmutzdecke develops, PM and chemical separation is improved with time. The "cake" can be easily removed through conventional maintenance.

In conclusion, this research investigates PA normally used for permeable pavement system through a physical modeling program of rainfall simulation, XRT and k and filtration mechanism modelling. The filtration mechanism model provided good agreement between measured and modeled results. A Computational Fluid Dynamics (CDF) model using a parametric analysis matrix of the pore structure and PM granulometric indices could yield a more detailed and comprehensive examination of filtration mechanisms and chemical load fate. A combination of parameter investigated by this research could be used to develop a combination CFD and machine learning (ML) model to predict PM separation and define maintenance routines and could be a follow up of this research.

Acknowledgements The authors acknowledge the contribution of the Eng. Matteo Brugin and Eng. Martina Ceriani through their graduation thesis, the AMALA laboratory at Politecnico di Milano and Capes for funding this work through the scholarship number BEX 9224/13-0.

Authors Contributions Conceptualization: M. Marchioni, R. Fedele, J. Sansalone, G. Becciu. Methodology: M. Marchioni, R. Fedele, J. Sansalone, G. Becciu. Formal analysis and investigation: M. Marchioni, R. Fedele, J. Sansalone, G. Becciu. Writing—original draft preparation: M Marchioni. Writing—review and editing: M. Marchioni, A. Raimondi. Supervision: G. Becciu.

Funding Open access funding provided by Politecnico di Milano within the CRUI-CARE Agreement. Capes through the scholarship number BEX 9224/13–0.

Availability of Data and Materials Authors agree with data transparency and undertake to provide any required data and material.

Declarations

Ethical Approval Not applicable.

Consent to Participate Not applicable.

Consent to Publish Not applicable.

Conflict of Interest The authors declare that they have no conflict of interest.

References

Alber S, Ressel W, Liu P, Hu J, Wang D, Oeser M, Uribe D, Steeb H (2018) Investigation of microstructure characteristics of porous asphalt with relevance to acoustic pavement performance, Int J Transport Sci Technol 7(3) ISSN 199–207:2046–2430. https://doi.org/10.1016/j.ijtst

Andrés-Valeri VC, Marchioni M, Sañudo-Fontaneda LA, Giustozzi F, Becciu G (2016) Laboratory assessment of the infiltration capacity reduction in clogged porous mixture surfaces. Sustainability 8(8):751
Auset M, Keller AA (2006) Pore-scale visualization of colloid straining and filtration in saturated porous media using micromodels. Water Resour Res 42(12)
Brugin M, Marchioni M, Becciu G, Giustozzi F, Toraldo E, Andrés-Valeri VC (2017) Clogging potential evaluation of porous mixture surfaces used in permeable pavement systems. Europ J Environm Civil Eng 1–11
CEN ECfS (2012) Bituminous Mixtures-Test method for hot mix asphalt Part 6: Test methods for hot mix asphalt. Determination of bulk density of bituminous specimens. BS EN 12697–6:2012
Chen J, Wang J, Wang H, Xie P, Guo L (2020) Analysis of Pore Characteristics and Flow Pattern of Open-Graded Asphalt Mixture in Different Directions. J Mater Civ Eng 32(9):04020256
Collins RE (1976) Flow of fluids through porous materials
Deletic A, Orr DW (2005) Pollution buildup on road surfaces. J Environ Eng 131(1):49–59
Dickenson JA, Sansalone JJ (2012) Distribution and disinfection of bacterial loadings associated with particulate matter fractions transported in urban wet weather flows. Water Res 46(20):6704–6714
Directive 2008/50/EC of the European Parliament and of the Council of 21 May 2008 on ambient air quality and cleaner air for Europe
Fedele R, Ciani A, Galantucci L, Bettuzzi M, Andena L (2013) A regularized, pyramidal multi-grid approach to global 3D-volume digital image correlation based on X-ray micro-tomography. Fund Inform 125(3–4):361–376
Huang W, Cai X, Li X, Cui W, Wu K (2020) Influence of nominal maximum aggregate size and aggregate gradation on pore characteristics of porous asphalt concrete. Materials 13(6):1355
IARC Working Group on the Evaluation of Carcinogenic Risks to Humans (2016) Outdoor Air Pollution. IARC Monogr Eval Carcinog Risks Hum 109:9
Kia A, Wong HS, Cheeseman CR (2017) Clogging in permeable concrete: A review. J Environ Manage 193:221–233
Kuang X, Ying G, Ranieri V, Sansalone J (2015) Examination of Pervious Pavement Pore Parameters with X-Ray Tomography. J Environ Eng 141(10):04015021
Li J, Deng C, Li Y et al (2017) Comprehensive Benefit Evaluation System for Low-Impact Development of Urban Stormwater Management Measures. Water Resour Manage 31:4745–4758. https://doi.org/10.1007/s11269-017-1776-5
Liu A, Li D, Liu L et al (2014) Understanding the Role of Urban Road Surface Characteristics in influencing Stormwater Quality. Water Resour Manage 28:5217–5229. https://doi.org/10.1007/s11269-014-0788-7
Lu G, Wang Z, Liu P, Wang D, Oeser M (2020) Investigation of the hydraulic properties of pervious pavement mixtures: characterization of Darcy and non-Darcy flow based on pore microstructures. Journal of Transportation Engineering, Part b: Pavements 146(2):04020012
Marchioni M, Becciu G (2015) Experimental Results On Permeable Pavements In Urban Areas: A Synthetic Review. Int J Sustain Dev Plan 10(6):806–817
Marchioni ML, Becciu G (2014) Permeable pavement used on sustainable drainage systems (SUDs): a synthetic review of recent literature. WIT Press Urban Water I I:12
Marchioni M, Fedele R, Raimondi A, Sansalone J, Becciu G (2021) Permeable Asphalt Hydraulic Conductivity and Particulate Matter Separation With XRT
McDowell-Boyer LM, Hunt JR, Sitar N (1986) Particle transport through porous media. Water Resour Res 22(13):1901–1921
Montes F, Valavala S, Haselbach LM (2005) A new test method for porosity measurements of Portland cement pervious concrete. J ASTM Int 2(1):1–13
Poulikakos LD, Sedighi Gilani M, Derome D, Jerjen I, Vontobel P (2013) Time resolved analysis of water drainage in porous asphalt concrete using neutron radiography, Applied Radiation and Isotopes, Volume 77. ISSN 5–13:0969–8043. https://doi.org/10.1016/j.apradiso.2013.01.040
Ranieri V, Antonacci MC, Ying G, Sansalone JJ (2010) Application of Kozeny-Kovàcs model to predict the hydraulic conductivity of permeable pavements. Transport Res Rec: J Transport Res (2195):168–176
Ranieri V, Colonna P, Sansalone JJ, Sciddurlo A (2012) Measurement of hydraulic conductivity in porous mixes. Transport Res Rec: J Transport Res Board (2295):1–10
Ranieri V, Berloco N, Colonna P, Fedele V, Sansalone JJ (2017a) Granulometry of Particulate Matter Recovered from Roadway Systems in Apulia (No. 17–05066)
Ranieri V, Berloco N, Colonna P, Fedele V, Sansalone JJ (2017b) Granulometry of Particulate Matter Recovered from Roadway Systems in Apulia. Transport Res Board 96th Annual Meeting (TRB). Washington DC, United States
Sansalone J, Cristina C (2004) Gradation-based metal mass prediction utilizing granulometry of snow particulate residuals. J Environ Eng 130(12):1488–1497.1410

Sansalone J, Ying G (2008) Partitioning and granulometric distribution of metal leachate from urban traffic dry deposition particulate matter subject to acidic rainfall and runoff retention. Water Res 42(15):4146–4162

Sansalone J, Tribouillard T (1999) Variation in characteristics of abraded roadway particles as a function of particle size: implications for water quality and drainage. Transport Res Rec: J Transport Res Board (1690):153–163

Sansalone J, Ying G, Lin H (2009) Distribution of metals for particulate matter transported in source area rainfall-runoff. J Environ Eng 136(2):172–184

Sansalone J, Kuang X, Ranieri V (2008) Permeable pavement as a hydraulic and filtration interface for urban drainage. J Irrig Drain Eng 134(5):666–674

Shepherd JM (2005) A review of current investigations of urban-induced rainfall and recommendations for the future. Earth Interact 9(12):1–27

Tansar H, Duan HF, Mark O (2022) Catchment-Scale and Local-Scale Based Evaluation of LID Effectiveness on Urban Drainage System Performance. Water Resour Manage. https://doi.org/10.1007/s11269-021-03036-6

Teng Z, Sansalone J (2004) In situ partial exfiltration of rainfall runoff. II: Particle separation. J Environ Eng 130(9):1008–1020

Tennis PD, Leming ML, Akers DJ (2004) Pervious concrete pavements, Portland Cement Association Skokie, IL

Terzaghi K, Peck RB, Mesri G (1996) Soil mechanics in engineering practice. John Wiley & Sons

Tsihrintzis VA, Hamid R (1997) Modeling and Management of Urban Stormwater Runoff Quality: A Review. Water Resour Manage 11:136–164. https://doi.org/10.1023/A:1007903817943

Ying G, Sansalone J (2010) Transport and solubility of Hetero-disperse dry deposition particulate matter subject to urban source area rainfall–runoff processes. J Hydrol 383(3–4):156–166

Zhang H, Sansalone J (2014) Partitioning and first-flush of nitrogen in rainfall-runoff from an urban source area. J Environ Eng 140(8):04014027